JOURNAL OF Applied Polymer SCIENCE

Long-range dipole–dipole energy transfer enhancement *via* addition of SiO_2/TiO_2 nanocomposite in PFO/MEH-PPV hybrid thin films

Bandar Ali Al-Asbahi,[1,2] **Saif M. H. Qaid**,[1,3] **Mohammad Hafizuddin Hj. Jumali**,[4] **Mohamad Saleh AlSalhi**,[1,5] **Abdullah S. Aldwayyan**[1,6]

[1]Department of Physics and Astronomy, College of Sciences, King Saud University, Riyadh 11451, Saudi Arabia
[2]Department of Physics, Faculty of Science, Sana'a University, Sana'a, Yemen
[3]Department of Physics, Faculty of Science, Ibb University, Ibb, Yemen
[4]School of Applied Physics, Faculty of Science and Technology, Universiti Kebangsaan Malaysia, UKM Bangi 43600, Selangor, Malaysia
[5]Research Chair in Laser Diagnosis of Cancers, College of Sciences, King Saud University, Riyadh 11451, Saudi Arabia
[6]King Abdullah Institute for Nanotechnology, King Saud University, Riyadh, Saudi Arabia
Correspondence to: B. A. Al-Asbahi (E-mail: balasbahi@ksu.edu.sa and alasbahibandar@gmail.com)

ABSTRACT: Different weight ratios of poly(9,9-dioctylfluorene-2,7-diyl) (PFO)/poly[2-methoxy-5-(2-ethylhexyloxy)-1,4-phenylenevinylene] (MEH-PPV) hybrid thin films, with and without a SiO_2/TiO_2 nanocomposite (NC), were successfully prepared using a solution blending method. All samples were deposited onto glass substrates by a spin coating technique to produce homogeneous thin films. The effect of the SiO_2/TiO_2 NC on the enhancement of the energy transfer mechanism in the PFO/MEH-PPV hybrids was investigated. The energy transfer parameters were calculated on the basis of the absorption and emission measurements. The long-range dipole–dipole energy transfer (Förster type) between the acceptor and donor molecules was enhanced in the presence of the SiO_2/TiO_2 NC in the hybrid thin films. The addition of the SiO_2/TiO_2 NC in the PFO/MEH-PPV hybrids reduced the distance between the donor and acceptor molecules more than the individual addition of SiO_2 or TiO_2 nanoparticles. Moreover, the direct relationships between the acceptor contents and energy transfer parameters, such as the energy transfer radius (R_{DA}), energy transfer efficiency (η), and energy transfer probability (P_{DA}), were estimated using theoretical fittings. © 2019 Wiley Periodicals, Inc. J. Appl. Polym. Sci. **2019**, *136*, 47845.

KEYWORDS: energy transfer; Förster-type; nanocomposite; PFO/MEH-PPV hybrids; thin films

Received 10 January 2019; accepted 31 March 2019
DOI: 10.1002/app.47845

INTRODUCTION

Organic materials with good emission responses are suitable candidates for numerous optoelectronic applications such as solar cells, photovoltaic sensors, and organic light-emitting diodes (OLEDs). In the solid state, conjugated organic combinations exhibit a unique variety of electrical, optical, and photoelectric properties.[1] Compared with inorganic materials, organic materials have numerous advantages, such as ease of processing and low cost. Moreover, inorganic nanostructures mixed with organic materials impart interesting and unique optoelectronic properties to nanocomposite (NC) materials.[2]

Although numerous conjugated organic light-emitting materials are highly luminescent in their dilute solutions, they become less emissive upon fabrication into thin films.[3] This reduction in their luminescence efficiency is attributed to the molecules aggregating and then forming less emissive species, such as excimers.[4] Phase separation, keto defect formation, and poor stability are other problems that can occur in the thin films of polymer blends owing to the low entropy of mixing between the dissimilar polymers and photooxidation during preparation of the film.[5–7] Many researchers have shown that these problems can be successfully reduced through several physical, chemical, and engineering methods.[8–10]

The solid state of the donor/acceptor combinations emits light; therefore, such combinations have attracted significant attention as the emissive layer in optoelectronic devices.[11–13] This enhancement in the emission of the solid state of the donor/acceptor combinations can be attributed to specific aggregation (J- or H-aggregation) or intramolecular planarization in the combinations.[8,14] Numerous models, such as rotational deactivation, noncoplanarity, and exciton diffusion, have been suggested for enhanced emission in the solid state compared with emission quenching in solutions.[15–17] Unfortunately, the intermolecular interaction occurs in the solid state of donor/acceptor blending, resulting in the quenching of the luminescence.[18] As reported in our previous study, this

problem can be diminished by incorporating inorganic nanomaterials.[12]

Several approaches have been utilized to enhance the OLED performance, including perfect matching between the working functions of the electrodes and the energy levels of the polymer,[19] multilayer device fabrication,[20] and utilization of hole and electron transporting layers.[20] Another recent technique involves the enhancement of Förster energy transfer.[21,22]

In our previous studies, the inclusion of TiO_2 NPs prevented the formation of dark quenchers and enhanced the emission performance.[10,12] Moreover, in a recent study, the visible and ultraviolet emission intensities of SiO_2/TiO_2 were greater than that of those of pure SiO_2 or TiO_2 NPs.[23] This enhancement in the emission intensities can be attributed the oxygen vacancies and trapped electrons at the interface of SiO_2/TiO_2 NC thin films.[23] Based on these findings, the incorporation of SiO_2/TiO_2 into the blends of the emitting polymers could improve the performance of optoelectronic devices through the enhanced Förster energy transfer.

Several strategies have been developed to prepare well-defined inorganic/organic hybrid NCs. The most common of these strategies are *via* starlike polymer as nanoreactors[24–26], sol–gel,[27] *in situ* polymerization,[28] and solution blending method.[29] In this study, poly (9,9′-di-n-octylfluorenyl-2.7-diyl) (PFO) as a donor and poly [2-methoxy-5-(2-ethyl-hexyloxy)-1,4-phenylenevinylene] (MEH-PPV) as an acceptor were blended at various ratios with and without a SiO_2/TiO_2 NC by the solution blending method. The ratio of SiO_2/20 wt. % TiO_2 was used in this study. The range used provided greater emission intensity than that of individual TiO_2 or SiO_2 NPs.[23] Then, thin-film blends were prepared by a spin coating technique. The optical properties and energy transfer mechanisms of these conjugated polymer hybrids were compared with and without the SiO_2/TiO_2 NC. The PFO/0.5 wt. % MEH-PPV hybrid was used to evaluate the effect of the individual addition of TiO_2 and SiO_2 NPs on this hybrid in terms of the optical properties and energy transfer mechanism. Furthermore, the effect of the acceptor content on the energy transfer parameters with and without the fixed ratio of the SiO_2/TiO_2 NC was evaluated by theoretical equations.

EXPERIMENTAL

PFO (Mw = 58,200 and PDI~ 3.7) and MEH-PPV (Mw = 40,000 and PDI ~ 6) were purchased from Sigma Aldrich (Saint Louis, Missouri, USA) and were used as received, without further purification. The chemical structures of these conjugated polymers are shown in Figure 1. The (SiO_2/20 wt. % TiO_2) was prepared as reported in our previous study, where the sizes of the TiO_2 and SiO_2 NPs were 25 and 26.4 nm, respectively.[23] The solution blending method was employed to prepare the PFO/MEH-PPV hybrid with various weight ratios of MEH-PPV: 0.1, 0.5, 1.0, 5.0, and 10 wt. %, with and without a fixed ratio of 10% SiO_2/(20% TiO_2) NC. The same procedures as those of our previous study were followed to prepare PFO/0.5 wt. % MEH-PPV with an individual fixed ratio of 10 wt. % TiO_2 and 10 wt. % SiO_2 NPs. All materials were dissolved in a toluene solvent produced by Fluka. This solvent produced a better distribution onto a glass substrate than that of other common solvents, such as THF. Here, 100 μL from each sample was deposited onto a glass substrate with the dimensions of 1.2 cm × 2 cm using a spin coating technique (2000 rpm for 20 s), and then, the samples were annealed at 120 °C in a vacuum oven to remove the solvent.

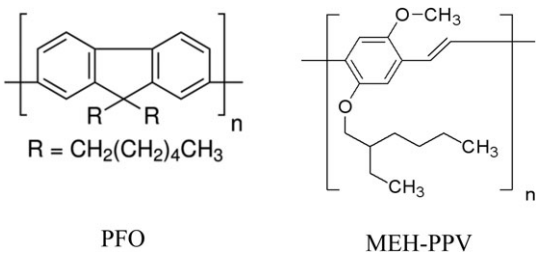

Figure 1. Chemical structure of PFO and MEH-PPV.

A Perkin Elmer Lambda 900 ultraviolet–visible Spectrometer was employed to obtain the absorption spectra, and an Edinburgh Instrument FLSP920 spectrophotometer was used to obtain the PL spectra and time resolved photoluminescence. Origin software (version 8.0) was used to analyze the absorption and emission data to determine the energy transfer parameters and to design the theoretical equations by fitting the curves.

RESULTS AND DISCUSSION

Absorption and Fluorescence Spectra

Figure 2(a) shows the absorption spectra of the thin films of pristine PFO, pristine MEH-PPV, and PFO with different contents of MEH-PPV, corresponding to 0.1, 0.5, 1.0, 5.0, and 10 wt. %. The absorbance peak of pristine PFO was in the range 300–450 nm with a maximum peak at approximately 398 nm, while two peaks were observed at 342 nm and 515 nm for pristine MEH-PPV. For the blended PFO with different contents of MEH-PPV, the peak at 342 nm was hidden, while the peak at 515 nm was enhanced dramatically with an increasing MEH-PPV content. Moreover, no new absorbance peak appeared upon increasing the MEH-PPV content up to 5 wt. %, indicating that no dimers formation of the hybrids were present. When the acceptor concentration was increased to 10 wt. %, a peak located at 515 nm was clearly observed due to molecules aggregation of MEH-PPV.

Figure 2(b) shows the emission spectra of pure PFO, pure MEH-PPV, and PFO with varying contents of MEH-PPV. With an excitation wavelength at 355 nm, three main peaks for PFO were observed at 437 nm, 458 nm, and 490 nm, corresponding to the 0-0, 0-1, and 0-2 vibronic transitions, respectively. Moreover, a shoulder peak at approximately 530 nm that was detected in the emission spectrum of pristine PFO was attributed to the formation of fluorenone defects (keto defects) in the PFO backbone during the photo-oxidation process.[2,7] Other peaks at 600 nm and 635 nm were observed for MEH-PPV, corresponding to the 0-0 and 0-1 transitions, respectively. The excitation wavelength of 355 nm was dominantly absorbed by the PFO. As MEH-PPV was added, the PFO intensity decreased significantly with a slight blue shift, while the intensity of the related peaks of MEH-PPV increased with a gradual red shift. This observation represented the energy transfer from PFO to MEH-PPV, as there was no major contribution from the MEH-PPV emission on the direct excitation at 355 nm in the region bellow 500 nm. The blue shift in the PFO emission was from the radiative energy transfer of the molecules of PFO (donor) to those of MEH-PPV (acceptor). The red shift in the MEH-PPV

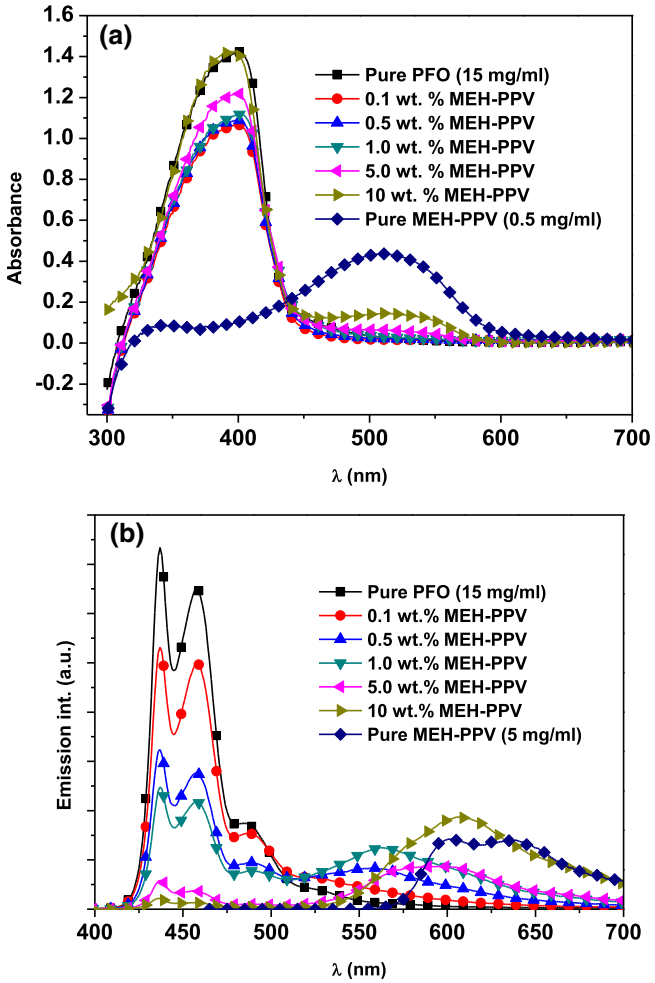

Figure 2. (a) Absorption spectra of pristine PFO, pristine MEH-PPV, and the hybrid thin films of PFO with different ratios (0.1, 0.5, 1.0, 5.0, and 10 wt. %) of MEH-PPV. (b) Emission spectra of pristine PFO, pristine MEH-PPV, and the hybrid thin films of PFO with different ratios (0.1, 0.5, 1.0, 5.0, and 10 wt. %) of MEH-PPV (λ_{ex} = 355 nm). [Color figure can be viewed at wileyonlinelibrary.com]

emission was attributed to the occurrence of radiative migration owing to self-absorption.[30] However, for a higher concentration of the acceptor, the energy migration among the molecules of PFO became minimal, and a direct transfer to the molecules of MEH-PPV, through the long-range dipole–dipole energy transfer (Förster-type) mechanism, occurred.

With the addition of 10 wt. % of (SiO_2/20 wt. % TiO_2) NC in the hybrids of PFO/diff. wt. % MEH-PPV, the maximum absorbance peak (398 nm) contained a blue shift to 15 nm. In addition, the absorbance peak of MEH-PPV in the ultraviolet (UV) region (342 nm) contained a blue shift to 295 nm (approximately 47 nm), and its intensity was significantly enhanced, as shown in Figure 3(a). A similar trend was observed with the addition of individual TiO_2 and SiO_2 NPs into the PFO/MEH-PPV hybrid (as shown later in Figure 4). The increase in the absorption peak of 295 nm with the addition of the SiO_2/TiO_2 NC to the PFO/MEH-PPV hybrids showed that the SiO_2/TiO_2 assisted the light harvesting in the UV region of 285–330 nm, and the surface area could be increased more than that with the addition of individual TiO_2 or SiO_2 NPs. Moreover, the large blue shift of the absorbance could be attributed to the nanoparticles producing a greater hindrance, thus reducing the conjugation lengths of the PFO and MEH-PPV, as described in the Critical Concentration of the Acceptor (Ao) and Conjugation Length (Aπ) section. This was consistent with the results obtained by Yang *et al.*,[31] where the absorption of the conjugated polymer in the NC contained a blue shift from the SiO_2 nanoparticles.

As shown in Figure 3(b), the addition of the SiO_2/TiO_2 NC enhanced the peak intensity corresponding to the acceptor and reduced that of the donor. Therefore, the SiO_2/TiO_2 NC facilitated the energy transfer between PFO and MEH-PPV. The energy transfer between the donor and the acceptor easily occurred with the SiO_2/TiO_2 NC owing to the stronger interactions Thus, with the SiO_2/TiO_2 NC, a small quantity from the acceptor could be used to acquire a long-range dipole–dipole

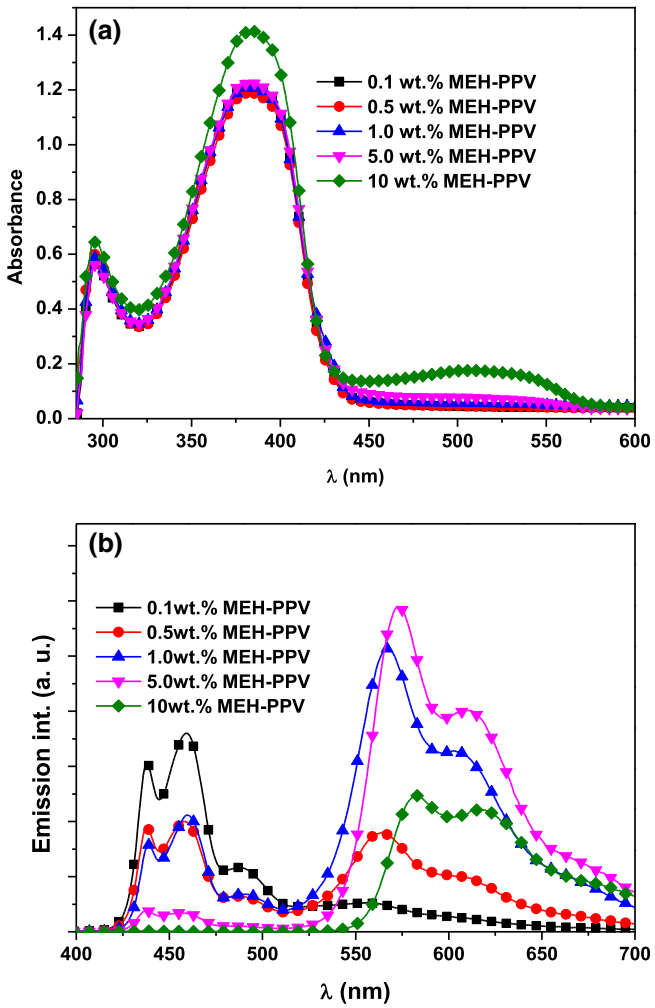

Figure 3. (a) Absorption spectra of the hybrid thin films of PFO with different ratios (0.1, 0.5, 1.0, 5.0, and 10 wt. %) of MEH-PPV with 10 wt. % (SiO_2/20 wt. % TiO_2) NC. (b) Emission spectra of the hybrid thin films of PFO with different ratios (0.1, 0.5, 1.0, 5.0, and 10 wt. %) of MEH-PPV with 10 wt. % (SiO_2/20 wt. % TiO_2) NC (λ_{ex} = 355 nm). [Color figure can be viewed at wileyonlinelibrary.com]

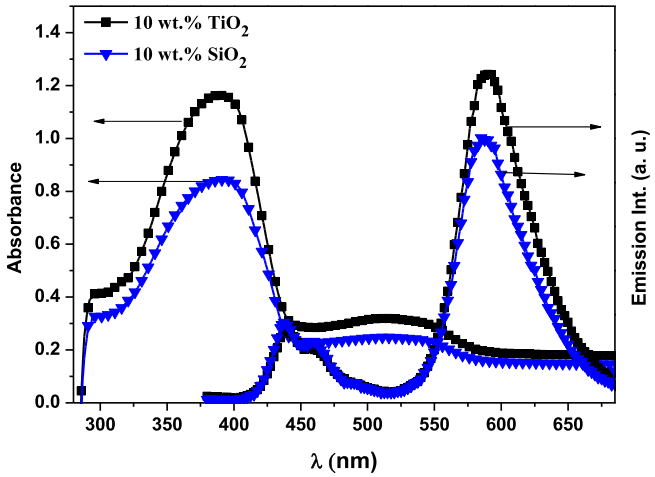

Figure 4. Absorption and emission spectra of PFO/0.5 wt. % MEH-PPV with 10 wt. % TiO_2 and 10 wt. % SiO_2 NPs. [Color figure can be viewed at wileyonlinelibrary.com]

energy transfer (Förster type) between the donor and the acceptor. This occurred even if the SiO_2 or TiO_2 was mixed individually with the PFO/MEH-PPV hybrid, as shown in Figure 4. However, for individual mixing, one peak related to the acceptor became dominant, while for mixing the SiO_2/TiO_2 NC, both peaks of the acceptor appeared. Because both peaks of the acceptor appeared for mixing the SiO_2/TiO_2 NC, the enhancement of the energy transfer should be greater than that of mixing individual SiO_2 or TiO_2 with the PFO/MEH-PPV hybrid. Even though both emission peaks were associated with the acceptor, the peaks of the donor remained at a high intensity. This enhancement in the emission intensity was attributed to the oxygen vacancies and charge trapping effect.[23,32]

An exciting phenomenon was observed at 10 wt. % MEH-PPV, where the emission intensity of the acceptor decreased instead of increasing, and the donor emission was simultaneously quenched. This quenching showed that the energy transfer process was completed, whereas the reduction in the emission intensity of the acceptor showed that the energy transfer from the donor to the significant number of acceptor molecules was not emitted as fluorescence. Instead the transferred energy was converted into heat, suggesting that some of the MEH-PPV molecules acted as dark quenchers without any fluorescence.[10] The dominant formation of the dark quenchers was attributed to the creation of nonfluorescent ground state complex dimers, as shown by the formation of the absorption peak (approximately 515 nm) at 10 wt. % in the absorption spectrum.

Long-Range Dipole–Dipole Energy Transfer Parameters

As shown in the emission spectra [Figure 2(b)], the energy transfer effect was clearly observed in the PFO/MEH-PPV hybrids when the acceptor content exceeded 0.1 wt. %. Moreover, this effect became more apparent when the SiO_2/TiO_2 NC was added into these hybrids, even with an acceptor content of 0.1 wt. % [Figure 3(b)]. To compare the energy transfer parameters for the PFO/MEH-PPV hybrids with and without the SiO_2/TiO_2 NC, an excitation wavelength of 355 nm was used, for which direct MEH-PPV excitation was insignificant, and energy transfer from PFO to MEH-PPV occurred. The possibility of long-range dipole–dipole energy transfer (Förster type) could be evidenced by (1) the strong overlap (not shown here) between the absorption spectrum of pristine MEH-PPV and the emission spectrum of pristine PFO, (2) the strong decrease in the emission intensity of PFO with the addition of MEH-PPV, and (3) the effective enhancement of the emission intensity of MEH-PPV. Several parameters, in the sections below, were evaluated to describe the energy transfer mechanism with and without the SiO_2/TiO_2 NC. Moreover, the ratio of PFO/0.5 wt. % MEH-PPV was employed to evaluate the effect of the individual addition of TiO_2 and SiO_2 on the energy transfer mechanism.

Quantum Yield and Lifetime of the Donor in the Hybrids. In homogeneous dynamic quenching, the following equation can be used to determine the quantum yield (φ_{DA}) and lifetime (τ_{DA}) values of the donor in the hybrid thin films:

$$\frac{I_D}{I_{DA}} = \frac{\emptyset_D}{\emptyset_{DA}} = \frac{\tau_D}{\tau_{DA}} \quad (1)$$

where I_D and I_{DA} are the emission intensity of donor in the absence and presence of acceptor, respectively.[11,33,34]

Table I lists the ϕ_{DA} and τ_{DA} values of PFO in the hybrid thin films, which decreased with the addition of MEH-PPV. This suggested the possibility of radiative energy transfer. The significantly shorter values of ϕ_{DA} and τ_{DA} than those of the pristine PFO thin film (ϕ_D = 0.72 and τ_D = 346 ps)[11] provided theoretical evidence of the efficient energy transfer from PFO to MEH-PPV. The values in Tables I and II were shorter with SiO_2 and TiO_2, as a mixture or an individual component, compared with those without SiO_2 and TiO_2 NPs. Moreover, this suggested that the efficient energy transfer with the SiO_2 and TiO_2 NPs was greater than that without the NPs, as discussed in the sections below.

Table I. Optical Properties of the Donor/Acceptor Thin Films with and without 10 wt. % (SiO_2/20 wt. % TiO_2)

In absence of SiO_2/TiO_2 NC					In presence of SiO_2/TiO_2 NC			
Acceptor content (wt. %)	ϕ_{DA}	K_{nr} $(ns)^{-1}$	A_π (Å)	τ_{DA} (ps)	ϕ_{DA}	K_{nr} $(ns)^{-1}$	A_π (Å)	τ_{DA} (ps)
0.1	0.521	1.905	0.087	251	0.354	3.802	–0.603	170
0.5	0.318	4.460	–0.764	153	0.195	8.569	–1.415	93.9
1.0	0.243	6.470	–1.135	117	0.207	7.949	–1.340	99.7
5.0	0.057	7.430	–2.801	27.53	0.035	56.39	–3.298	17.1
10	0.021	9.630	–3.842	10.08	0.004	505.5	–5.492	1.97

Table II. Energy Transfer Parameters of the PFO/0.5 wt. % MEH-PPV Hybrid Thin Film with SiO2 and TiO2

Dopant (10 wt. %)	ϕ_{DA}	τ_{DA} (ps)	R_0 (Å)	R_{DA} (Å)	k_{ET} $(ns)^{-1}$	A_π (Å)	A_O (mM)
TiO_2	0.144	69.2	84.2	66.8	11.5	−1.782	0.75
SiO_2	0.216	104	84.7	73.5	6.74	−1.289	0.73

Stern–Volmer (k_{SV}) and Quenching Rate (k_q) Constants. The homogeneity of the dynamic quenching of PFO by MEH-PPV with and without the SiO_2/TiO_2 NC was determined from the linear Stern–Volmer plot (Figure 5). The values of k_{SV}, with and without the SiO_2/TiO_2 NC, were 4.21 and 0.78 $(\mu M)^{-1}$, respectively. These values implied that 50% of the fluorescence was quenched for the MEH-PPV concentrations of approximately 0.24 and 1.28 μM with and without the SiO_2/TiO_2 NC, respectively.

The value of k_q with the SiO_2/TiO_2 NC was 1.22×10^{16} M^{-1} s^{-1}, approximately five times greater than that without the SiO_2/TiO_2 NC (2.25×10^{15} M^{-1} s^{-1}). The high values of k_q are indicated of how well mixing between the conjugated polymers and the SiO_2/TiO_2 NCs.[34]

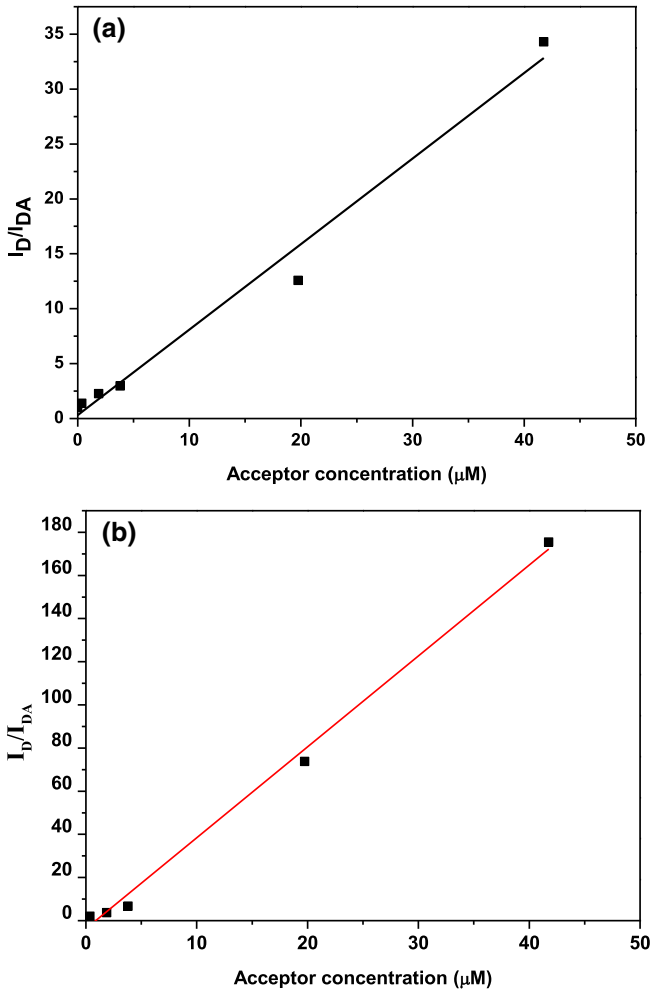

Figure 5. Stern–Volmer plots for emission quenching of PFO by various weight ratios of MEH-PPV: (a) without SiO_2/20 wt. % TiO_2 and (b) with 10 wt. % (SiO_2/20 wt. % TiO_2). [Color figure can be viewed at wileyonlinelibrary.com]

Förster Radius, Energy Transfer Rate, and Energy Transfer Lifetime. The critical distance (Förster radius), R_0, is calculated from the following formula.[35]

$$R_o^6 = \frac{9000(\ln 10)\beta^2\phi_D}{128\pi^5 n^4 N_o}\int F_D(\lambda)\varepsilon_A(\lambda)\lambda^4 d\lambda = \frac{9000(\ln 10)\beta^2\phi_D}{128\pi^5 n^4 N_o} J(\lambda) \quad (2)$$

The parameter β^2 is the orientation factor (2/3 for isotropic media), and n is the refractive index of the solvent. The parameter N_o is Avogadro's number and λ is the wavelength. The parameter $\varepsilon_A[\lambda]$ is the molar decadic extinction coefficient of the acceptor, and F_D (λ) is the normalized spectral distribution of the donor (i.e., $\int F_D(\lambda)\, d\lambda = 1$). The values of R_o and $J(\lambda)$ with and without the SiO_2/TiO_2 NC are listed in Table III. The values of R_o and $J(\lambda)$ with the SiO_2/TiO_2 NC were slightly larger than those without the NC. The Förster radii with and without the SiO_2/TiO_2 NC were in the ranges of 48–89 and 43–87 Å, respectively. These values confirmed the dominant long-range dipole–dipole energy transfer (Förster type) in the hybrids.[36,37] Consequently, the Förster theory is suitable for calculating the Förster energy transfer parameters, as previously reported.[38–40] Moreover, the values of R_o with individual SiO_2 and TiO_2 in the hybrid of PFO/0.5 wt. % MEH-PPV were 84.7 and 84.2 Å, respectively. This was because the particle sizes of SiO_2 and TiO_2 were approximately the same, and thus, the surface area was similar. The decreasing of R_o (approximately 77.7 Å) when mixing PFO/0.5 wt. % MEH-PPV with the SiO_2/TiO_2 NC could be attributed to the defect formation and the surface area increase, as discussed previously in the Absorption and Fluorescence Spectra section. Based on the R_o values, the mechanism of the Förster energy transfer is suitable in the PFO/MEH-PPV system with SiO_2 and TiO_2 as a mixture or individual compounds.

The calculation of the distance between the donor and acceptor molecules (R_{DA}) was based on the Förster radius and fluorescence intensities of the donor without (I_D) and with (I_{DA}) the acceptor. Figure 6 shows that as the acceptor content increased from 0.1 to 10 wt. %, the R_{DA} decreased from 105 to 24 Å and from 87 to 22 Å, without and with the SiO_2/TiO_2 NC, respectively. This implied that the distance between the molecules of PFO and MEH-PPV became smaller with the SiO_2/TiO_2 NC. Furthermore, a reduction in the values of R_{DA} was detected even if the SiO_2 or TiO_2 NPs were added individually in the PFO/MEH-PPV hybrid (Table II); however, this reduction was not less than that of the hybrid with the mixture of SiO_2/TiO_2.

Table III. Energy Transfer Parameters of the Donor/Acceptor Thin Films with and without 10 wt. % (SiO_2/20 wt. % TiO_2)

	In absence of SiO_2/TiO_2 NC						In presence of SiO_2/TiO_2 NC					
Acceptor content (wt. %)	$J(\lambda) \times 10^{15}$ (M^{-1} cm^{-1} nm^4)	R_0 (Å)	R_{DA} (Å)	k_{ET} $(ns)^{-1}$	τ_{ET} (ps)	TDR $(ns)^{-1}$	$J(\lambda) \times 10^{15}$ (M^{-1} cm^{-1} nm^4)	R_0 (Å)	R_{DA} (Å)	k_{ET} $(ns)^{-1}$	τ_{ET} (ps)	TDR $(ns)^{-1}$
0.1	51.8	87.1	105.4	1.10	1184	3.99	61.5	89.7	86.6	2.99	219	5.88
0.5	9.33	65.5	65.9	3.66	237	6.55	26.1	77.7	62.98	7.76	43.8	10.7
1.0	6.11	61.5	60.2	5.66	117	8.55	13.9	70.0	54.56	7.14	21.6	10.0
5.0	1.67	49.2	32.7	33.4	22.5	36.3	2.10	51.1	31.20	55.5	4.16	58.4
10	0.82	43.7	24.3	96.2	10.6	99.1	1.40	47.7	22.07	504	1.97	507

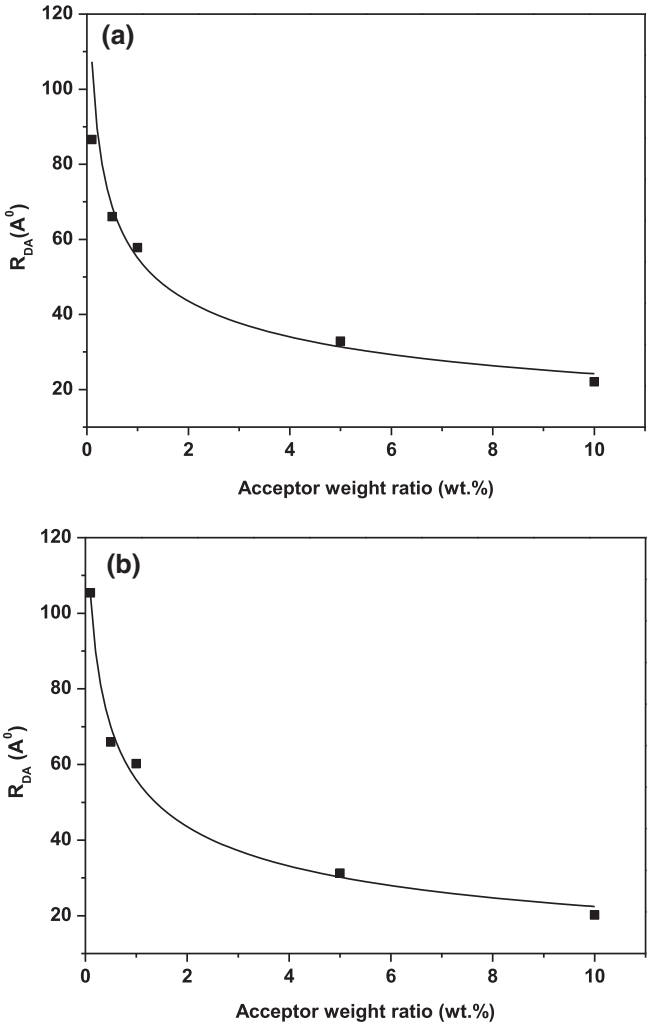

Figure 6. Distance between the molecules of the donor/acceptor versus the acceptor content: (a) without SiO_2/20 wt. % TiO_2 and (b) with 10 wt. % (SiO_2/20 wt. % TiO_2).

The reduction in R_{DA} with the NPs was consistent with previous results of PFO/Fluorol 7GA with TiO_2 NPs.[34] Moreover, by fitting the data of Figure 6, theoretical equations were obtained to provide the relationships between R_{DA} and the acceptor content as follows.

$$R_{DA} = \left(0.00387 + 0.0143X^{0.418}\right)^{-1} \quad (3)$$

The parameter X is the acceptor weight ratio (wt. %) without the SiO_2/TiO_2 NC.

$$R_{DA} = \left(0.006 + 0.0127X^{0.506}\right)^{-1} \quad (4)$$

The parameter X is the acceptor weight ratio (wt. %) with the SiO_2/TiO_2 NC.

The energy transfer rate (k_{ET}) between a single donor/acceptor pair separated by a distance between the donor and acceptor (R_{DA}) can be expressed in terms of the Förster distance (R_0).[41]

$$k_{ET} = \frac{1}{\tau_D}\left(\frac{R_o}{R_{DA}}\right)^6 \quad (5)$$

As listed in Table III, the R_{DA} values were significantly smaller than those without the SiO_2/TiO_2 NC; whereas, the changes in the R_0 values were insignificant compared with those without the SiO_2/TiO_2 NC. Consequently, the energy transfer rate (k_{ET}) values were enhanced with SiO_2 and TiO_2, as a mixture or individual compounds, in the hybrids (Tables II and III).

The variations in the values of the energy transfer lifetime (τ_{ET}), energy transfer rate (k_{ET}), and total decay rate (TDR) of the donor ($k_{ET} + \tau_D^{-1}$) with the addition of the SiO_2/TiO_2 NC in the hybrid thin films with various acceptor contents are listed in Table III. As shown in previous studies,[11,33,34] an efficient energy transfer in the donor/acceptor hybrids is shown by an increase in the k_{ET} and TDR and a decrease of τ_{ET} with an increasing acceptor content. These findings were observed in the current system of the donor/acceptor hybrids. In the presence of the SiO_2/TiO_2 NC, the values of τ_{ET} were approximately five times smaller, whereas the values of k_{ET} and the TDR were larger than those without the SiO_2/TiO_2 NC. This showed the positive effect of the SiO_2/TiO_2 NC on the enhancement of the long-range dipole–dipole energy transfer (Förster type) between PFO and MEH-PPV.

The Probability (P_{DA}) and Efficiency (η) of the Donor/Acceptor Energy Transfer. Figures 7 and 8 show the relationship of the acceptor content with P_{DA} and η, respectively. A gradual increase occurred for P_{DA} with the addition of the acceptor with and without the SiO_2/TiO_2 NC. The larger increase in the P_{DA} values in the presence of the SiO_2/TiO_2 NC was attributed to the systematic reduction in the emission intensity (I_{DA}) that was greater than that without the SiO_2/TiO_2 NC. Moreover, by fitting the data of Figure 7, the relationships between P_{DA} and the acceptor content with and without the SiO_2/TiO_2 NC were as follows.

$$P_{DA} = e^{(22.07 + 0.57X - 0.024X^2)} \quad (6)$$

The parameter X is the acceptor weight ratio (wt. %) without the SiO_2/TiO_2 NC.

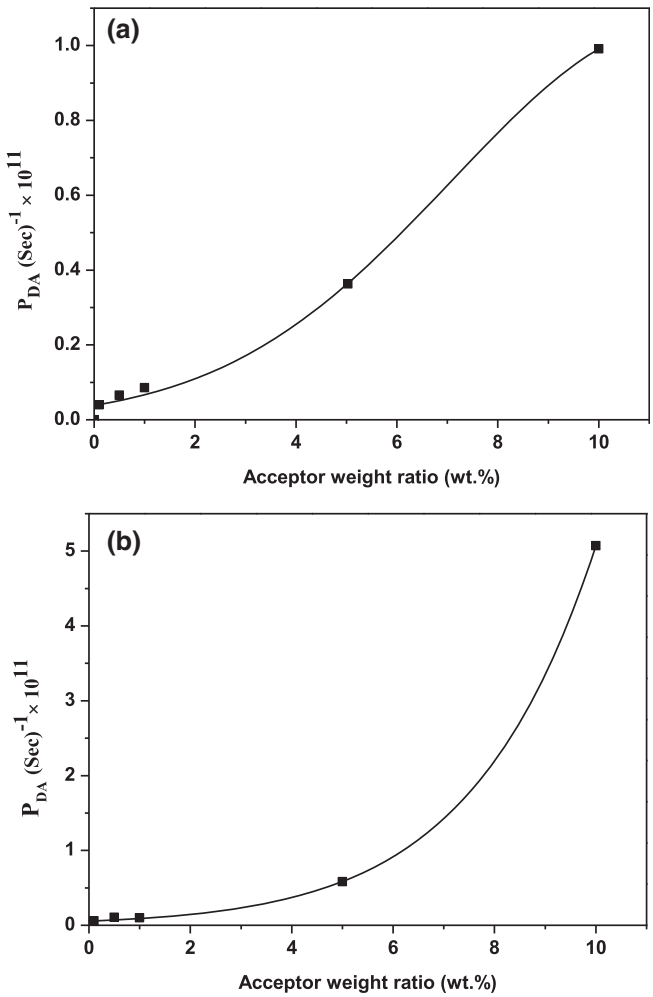

Figure 7. Probability of the energy transfer from PFO to MEH-PPV for various weight ratios: (a) without SiO_2/20 wt. % TiO_2 and (b) with 10 wt. % (SiO_2/20 wt. % TiO_2).

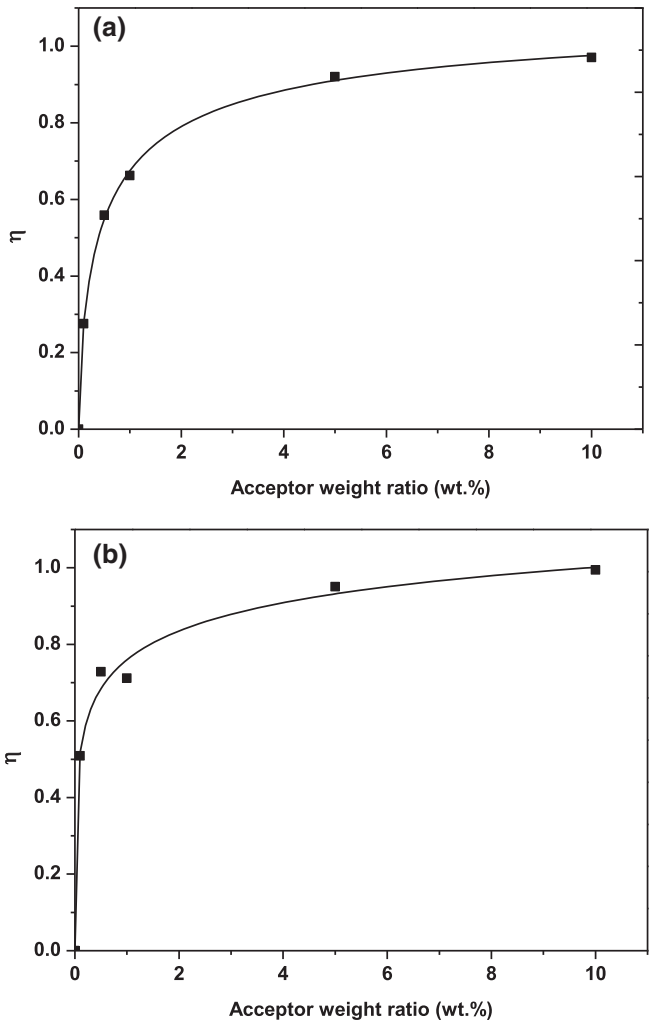

Figure 8. Efficiency of the energy transfer from PFO to MEH-PPV for various weight ratios: (a) with SiO_2/20 wt. % TiO_2 and (b) without 10 wt. % (SiO_2/20 wt. % TiO_2).

$$P_{DA} = e^{(22.42 + 0.49X - 0.004X^2)} \quad (7)$$

The parameter X is the acceptor weight ratio (wt. %) with the SiO_2/TiO_2 NC.

A systematic increase in the energy transfer efficiency (η) was observed until the acceptor content reached 5 wt. % with and without the SiO_2/TiO_2 NC, as shown in Figure 8. The maximum energy transfer efficiencies without and with the SiO_2/TiO_2 NC were 0.97 and 0.99, respectively. This also showed the positive effect of the SiO_2/TiO_2 NC in the blends to enhance the mechanism of the energy transfer between PFO and MEH-PPV. By fitting the data of Figure 8, the relationship between η and the acceptor content with and without the SiO_2/TiO_2 NC was estimated as follows.

$$\eta = \frac{1.11X^{0.67}}{0.64 + X^{0.67}} \quad (8)$$

The parameter X is the acceptor weight ratio (wt. %) without the SiO_2/TiO_2 NC.

$$\eta = \frac{1.51X^{0.29}}{0.98 + X^{0.29}} \quad (9)$$

The parameter X is the acceptor weight ratio (wt. %) with the SiO_2/TiO_2 NC.

As shown in Figure 9, an inflection point in η was observed at $R_{DA} = R_o$. The parameter η was close to unity at $R_{DA} < 0.5\ R_o$ and dramatically decreased for $R_{DA} > R_o$. Therefore, the long-range dipole–dipole energy transfer (Förster type) from PFO, with and without the SiO_2/TiO_2 NC, to MEH-PPV occurred at a higher probability for 10 Å < R_o < 100 Å. Moreover, the distance between the PFO and MEH-PPV molecules was less than 1.5 R_o. These results are consistent with previous reports.[11,34,42]

Critical Concentration of the Acceptor (A_o) and Conjugation Length (A_π). The concentration of the acceptor with 76% energy transfer is the critical concentration (A_o).[33] The concentration of the acceptor should be much lower than A_o to suppress the intermolecular

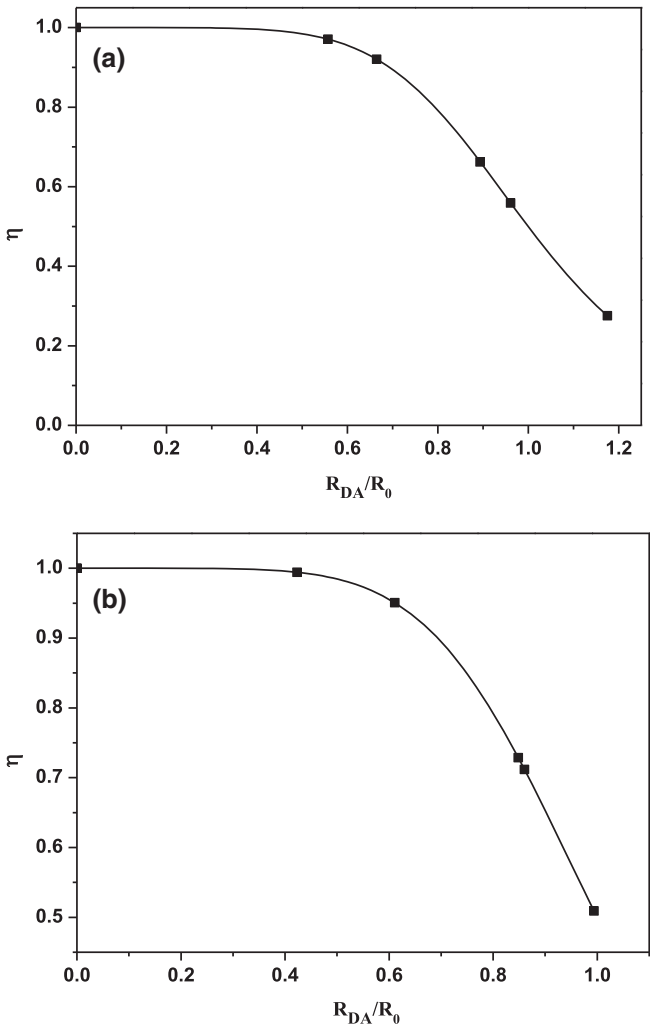

Figure 9. Dependence of the efficiency of the energy transfer (η) on the distance between the molecules of the donor/acceptor: (a) without SiO_2/20 wt. % TiO_2 and (b) with 10 wt. % (SiO_2/20 wt. % TiO_2).

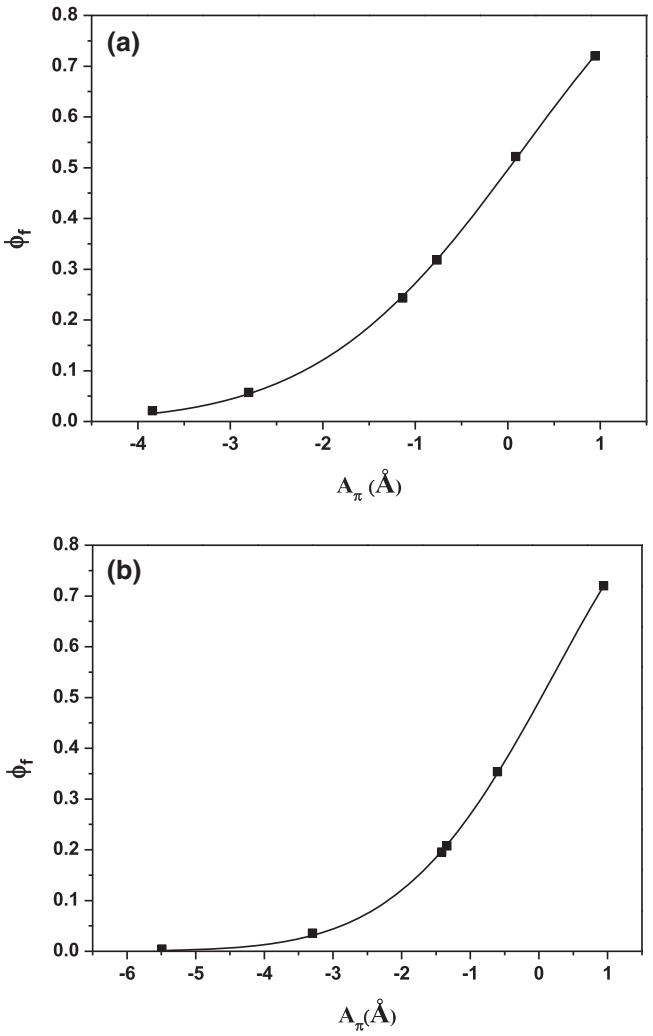

Figure 10. Fluorescence quantum yield (Φ_{DA}) versus the conjugated length (A_π): (a) without SiO_2/20 wt. % TiO_2 and (b) with 10 wt. % (SiO_2/20 wt. % TiO_2).

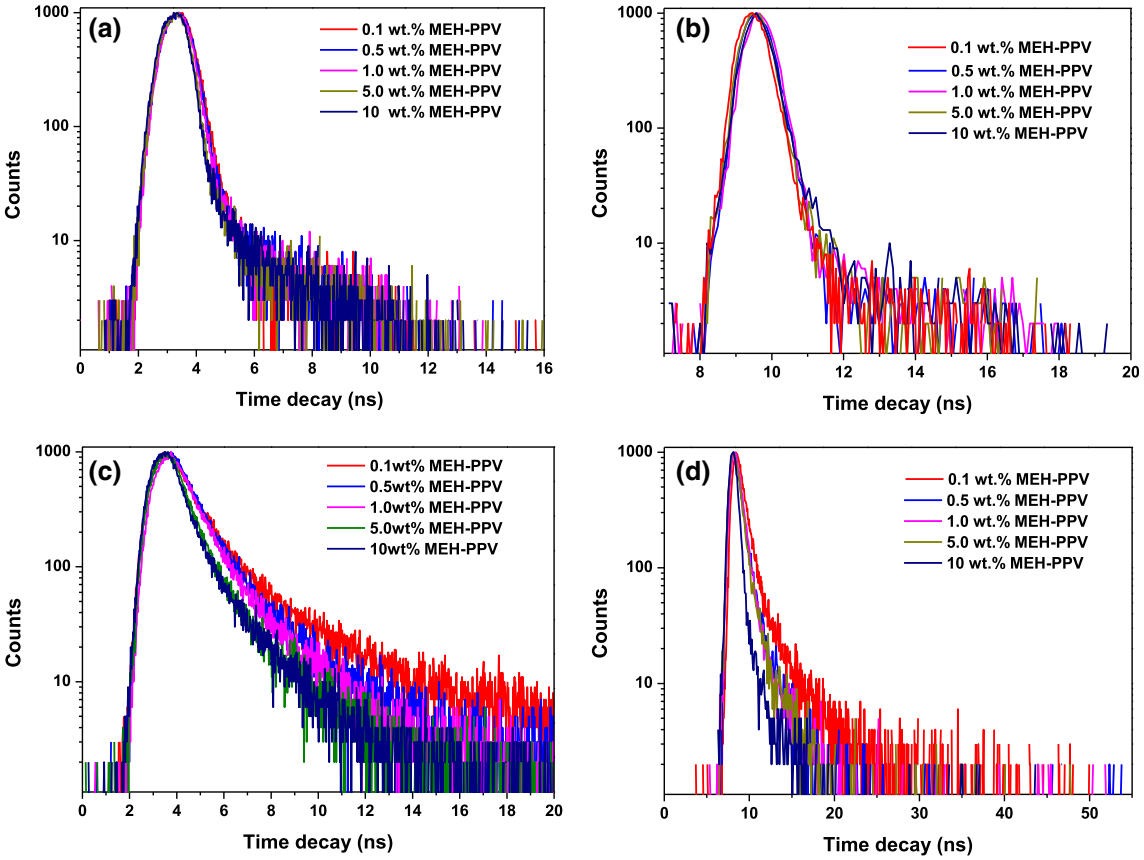

Figure 11. Lifetime decays at λ_{em} = 440 nm: (a) without SiO_2/20 wt. % TiO_2 and (b) with 10 wt. % (SiO_2/20 wt. % TiO_2) and Lifetime decays at λ_{em} = 560 nm: (c) without SiO_2/20 wt. % TiO_2 and (d) with 10 wt. % (SiO_2/20 wt. % TiO_2). [Color figure can be viewed at wileyonlinelibrary.com]

transfer in the donor. Based on the R_0 values, the A_o values of MEH-PPV were approximately 0.62 and 0.67 mM, without and with the SiO_2/TiO_2 NC, respectively, while these values increased to 0.73 and 0.75 mM with SiO_2 and TiO_2, respectively.

The conjugation length (A_π) value in the excited singlet state is defined as the distance between the dipoles arising from the ground state (S_0) to the excited singlet state (S_1) transition, derived from the radiative rate constant (k_r) and radiationless rate constant (k_{nr}). There was no significant modification in the value of k_r (approximately 2.08 ns^{-1}) with the increase of the acceptor content, even in the presence of the SiO_2/TiO_2 NC. However, the value of k_{nr} significantly increased with an increasing acceptor concentration, and it was greater with the SiO_2/TiO_2 NC. Consequently, A_π decreased for an increasing acceptor concentration, with a smaller value with the SiO_2/TiO_2 NC than that without the NC. The values of A_π with and without the SiO_2 and TiO_2 NPs, as a mixture and individual components, are listed in Tables I and II. The decrease in the R_{DA} and A_π values with the SiO_2 and TiO_2, as a mixture or individual components, showed that SiO2 and TiO_2 reduced the distance between the PFO and MEH-PPV molecules.

Figure 10 shows the exponential relationship between Φ_{DA} and A_π. This relationship showed that the addition of the NC could produce organic compounds that were highly fluorescent. There was an approximately linear portion when Φ_{DA} exceeded 0.25 and 0.19 without and with the SiO_2/TiO_2 NC, respectively. As shown in Figure 10, when $\Phi_{DA} \sim 0.5$, $A_\pi = 0$ [where $k_r = k_{nr}$ from $\Phi_f = k_r/(k_r + k_{nr})$]. Moreover, for a decrease in A_π, Φ_{DA} decreased.

Lifetime Decay

The lifetime decay (mean/average fluorescence lifetime) differed from the fluorescence lifetime (in Table I). The lifetime decay includes the radiative emission, while the fluorescence lifetime includes the radiative emission and nonradiative emission.[43] The lifetime decays obtained at 440 nm for the PFO/MEH-PPV hybrids with and without the SiO_2/TiO_2 NC, corresponding to the emission region of PFO, are shown in Figure 11(a,b), respectively. The acceptor decays for the PFO/MEH-PPV hybrids with and without the SiO_2/TiO_2 NC at a collection wavelength of 560 nm are shown in Figure 11(c,d), respectively. A global analysis including the data obtained at 440 and 560 nm was also carried out, confirming the general trends of the data in Tables IV and V. In these tables, the lifetime decays were calculated by the following expression.

$$\tau = \frac{\sum_i (\tau_i^2 B_i)}{\sum_i (\tau_i B_i)} \quad (10)$$

The parameters B_i and τ_i are the fitting parameters, which are strongly dependent on the conformer geometries and environment. The existence of one, two, or three lifetimes can be interpreted by the presence of one, two, or three conformers.[44] This allows a comparison between the various decays and the realization

Table IV. Main Fitting Parameters And Lifetime Decays of the Thin Films of PFO at 0.1, 0.5, 1.0, 5.0, and 10 wt. % of MEH-PPV

At $\lambda_{em.}$ 440 nm				At $\lambda_{em.}$ 560 nm							
Acceptor content (wt. %)	Relative amplitude	Donor lifetime		Acceptor lifetime (ps)			Relative amplitude				
	B	τ (ps)	χ^2	τ_1	τ_2	τ_3	B_1	B_2	B_3	τ (ps)	χ^2
0.1	0.131	174	0.767	358	1128	5228	0.021	0.021	0.001	1557	1.232
0.5	0.131	160	0.800	920	3394	-	0.034	0.002	-	1361	1.565
1.0	0.168	117	0.737	827	2678	-	0.032	0.002	-	1138	0.964
5.0	0.290	63	0.924	581	1981	-	0.033	0.003	-	912	1.104
10	0.316	59	1.784	461	1766	-	0.049	0.004	-	772	1.138

Table V. Main fitting parameters and lifetime decays of the thin films of PFO at 0.1, 0.5, 1.0, 5.0, and 10 wt. % MEH-PPV with 10 wt. % (SiO2/20 wt. % TiO2)

At $\lambda_{em.}$ 440 nm				At $\lambda_{em.}$ 560 nm					
	Relative amplitude	Donor lifetime		Relative amplitude		Acceptor lifetime (ps)			
Acceptor content (wt. %)	B	τ (ps)	χ^2	B_1	B_2	τ_1	τ_2	τ (ps)	χ^2
0.1	0.432	116	1.095	0.101	0.005	658	311	650	1.269
0.5	1.354	46	1.122	0.988	0.067	62	955	518	0.817
1.0	1.354	44	1.057	0.220	-	-	-	588	0.787
5.0	1.668	31	0.947	0.224	-	-	-	596	0.883
10	1.213	47	0.816	0.460	-	-	-	224	0.929

of the influence of the acceptor content on the hybrids with and without the SiO_2/TiO_2 NC. From these tables, there were faster decays at 440 nm with increased acceptor contents, which was a result of the more efficient energy transfer to the acceptor molecules with the SiO_2/TiO_2 NC, than that without the SiO_2/TiO_2 NC. This is consistent with the previous observations of the emission spectra in Figures 2(b) and 3(b). Moreover, this is in agreement with the results obtained by Cury and coworkers for PFO/MEH-PPV blends.[45]

The offset between the energy levels for the MEH-PPV and PFO[46,47] suggested an exciplex formation between the donor and the acceptor. Therefore, the long decay component in the MEH-PPV emission decay at 560 nm was attributed to the presence of the exciplex, which is in agreement with a previous report for the PFO/MEH-PPV blend.[45] As shown in Figures 2(b) and 3(b), the difference in the blue shifts with the peak position of the MEH-PPV, with and without the SiO_2/TiO_2 NC, were attributed to the overlap of the exciplex and the MEH-PPV emission.[45]

CONCLUSION

Thin films of the PFO/MEH-PPV hybrids with and without the SiO_2/TiO_2 NC were investigated by absorption, steady-state photoluminescence, and time-resolved photoluminescence at room temperature. Strong long-range dipole–dipole energy transfer (Förster-type) effects from the PFO to the MEH-PPV were confirmed. This study confirmed that the addition of the SiO_2/TiO_2 NC influenced the energy transfer properties of the thin films owing to the stronger interactions between the PFO and MEH-PPV molecules in the confined NC than those of bulk thin films. The maximum energy transfer efficiencies without and with the SiO_2/TiO_2 NC were 0.97 and 0.99, respectively, at 5 wt. % MEH-PPV. This improved Förster-type energy transfer with the SiO_2/TiO_2 NC, compared with that without the NC, was shown by the faster reduction in the quantum yields, lifetime decays, and lifetime energy transfers. Moreover, the conjugation length of the PFO was smaller with the addition of MEH-PPV and the SiO_2/TiO_2 NC than that without the NC. Moreover, the addition of TiO_2 NPs to the PFO/MEH-PPV hybrid provided a greater enhancement of the optical properties and energy transfer mechanism than that of the SiO_2 NPs. Although the addition of the TiO_2 NPs into the PFO/MEH-PPV hybrid reduced ϕ_{DA}, τ_{DA}, and A_π more than those with the SiO_2 or SiO_2/TiO_2 NC. The SiO_2/TiO_2 NC showed the largest reduction in the distance between the donor and acceptor molecules. The relationships between the acceptor content with R_{DA}, η, and P_{DA} were successfully represented by theoretical equations with and without the SiO_2/TiO_2 NC. The influence of the varying ratio of the SiO_2/TiO_2 NC on the best ratio of PFO/MEH-PPV will be evaluated in future studies to enhance the efficiency of the emissive layer in OLEDs.

ACKNOWLEDGMENTS

The authors extend their appreciation to the Deanship of Scientific Research at King Saud University for funding this work through research group No (RG-1440-037).

REFERENCES

1. Sheats, J. R.; Barbara, P. F. *Acc. Chem. Res.* **1999**, *32*, 191.
2. Al-Asbahi, B. A.; Jumali, M. H. H.; Yap, C. C.; Salleh, M. M. *J. Nanomater.* **2013**, *130*, 2013.
3. Friend, R.; Gymer, R.; Holmes, A.; Burroughes, J.; Marks, R.; Taliani, C.; Bradley, D.; Dos Santos, D.; Bredas, J.; Lögdlund, M. *Nature*. **1999**, *397*, 121.
4. Jenekhe, S. A.; Osaheni, J. A. *Science*. **1994**, *265*, 765.
5. Chappell, J.; Lidzey, D. G.; Jukes, P. C.; Higgins, A. M.; Thompson, R. L.; O'Connor, S.; Grizzi, I.; Fletcher, R.; O'Brien, J.; Geoghegan, M. *Nat. Mater.* **2003**, *2*, 616.
6. Geoghegan, M.; Krausch, G. *Prog. Polym. Sci.* **2003**, *28* (261), 261.
7. List, E. J.; Guentner, R.; Scanducci de Freitas, P.; Scherf, U. *Adv. Mater.* **2002**, *14*, 374.
8. Chen, J.; Xu, B.; Ouyang, X.; Tang, B. Z.; Cao, Y. *J. Phys. Chem. A*. **2004**, *108*, 7522.
9. Panthi, K.; Adhikari, R. M.; Kinstle, T. H. *J. Phys. Chem. A*. **2010**, *114*, 4542.
10. Al-Asbahi, B. A.; Jumali, M. H. H.; Yap, C. C.; Salleh, M. M.; AlSalhi, M. S. *Chem. Phys. Lett.* **2013**, *570*, 109.
11. Al-Asbahi, B. A.; Jumali, M. H. H.; Yap, C. C.; Flaifel, M. H.; Salleh, M. M. *J. Lumin.* **2013**, *142*, 57.
12. Al-Asbahi, B. A.; Haji Jumali, M. H.; AlSalhi, M. S. *Polymers*. **2016**, *8*, 334.
13. Chen, C.-T. *Chem. Mater.* **2004**, *16*, 4389.
14. Chen, H.; Lam, W.; Luo, J.; Ho, Y.; Tang, B.; Zhu, D.; Wong, M.; Kwok, H. S. *Appl. Phys. Lett.* **2002**, *81*, 574.
15. Chen, J.; Law, C. C.; Lam, J. W.; Dong, Y.; Lo, S. M.; Williams, I. D.; Zhu, D.; Tang, B. Z. *Chem. Mater.* **2003**, *15*, 1535.
16. Chen, J.; Xie, Z.; Lam, J. W.; Law, C. C.; Tang, B. Z. *Macromolecules*. **2003**, *36*, 1108.
17. An, B.-K.; Kwon, S.-K.; Jung, S.-D.; Park, S. Y. *J. Am. Chem. Soc.* **2002**, *124*, 14410.
18. Wang, R.; Shi, Z.; Zhang, C.; Zhang, A.; Chen, J.; Guo, W.; Sun, Z. *Dyes Pigm.* **2013**, *98*, 450.
19. Godlewski, J. *Adv. Colloid Interface Sci.* **2005**, *116*, 227.
20. Lu, J.; Tao, Y.; D'iorio, M.; Li, Y.; Ding, J.; Day, M. *Macromolecules*. **2004**, *37*, 2442.
21. Zhang, D.; Cai, M.; Zhang, Y.; Bin, Z.; Zhang, D.; Duan, L. *ACS Appl. Mater. Interfaces*. **2016**, *8*, 3825.
22. Guzelturk, B.; Demir, H. V. *Adv. Funct. Mater.* **2016**, *26*, 8158.
23. Al-Asbahi, B. A. *Mater. Res. Bull.* **2017**, *89*, 286.
24. Chen, Y.; Wang, Z.; He, Y.; Yoon, Y. J.; Jung, J.; Zhang, G.; Lin, Z. *Proc. Natl. Acad. Sci.* **2018**, *115*, E1391.
25. Chen, Y.; Yoon, Y. J.; Pang, X.; He, Y.; Jung, J.; Feng, C.; Zhang, G.; Lin, Z. *Small.* **2016**, *12*, 6714.
26. Li, X.; Iocozzia, J.; Chen, Y.; Zhao, S.; Cui, X.; Wang, W.; Yu, H.; Lin, S.; Lin, Z. *Angew. Chem. Int. Ed.* **2018**, *57*, 2046.
27. Catauro, M.; Papale, F.; Piccirillo, G.; Bollino, F. *Polym. Eng. Sci.* **2017**, *57*, 478.
28. Adnan, M.; Dalod, A.; Balci, M.; Glaum, J.; Einarsrud, M.-A. *Polymers*. **2018**, *10*, 1129.
29. Al-Asbahi, B.; Haji Jumali, M.; AlSalhi, M. *Polymers*. **2016**, *8*, 334.
30. Sahare, P.; Sharma, V. K.; Mohan, D.; Rupasov, A. *Spectrochim. Acta A Mol. Biomol. Spectrosc.* **2008**, *69*, 1257.
31. Yang, S.; Nguyen, T.; Le Rendu, P.; Hsu, C. *Compos. Part A Appl. Sci. Manuf.* **2005**, *36*, 509.
32. Jumali, M. H. H.; Al-Asbahi, B. A.; Yap, C. C.; Salleh, M. M.; Alsalhi, M. S. *Thin Solid Films*. **2012**, *524*, 257.
33. Lakowicz, J. R. Principles of Fluorescence Spectroscopy; Springer: London, **2009**.
34. Al-Asbahi, B. A. *Opt. Mater.* **2017**, *72*, 644.
35. Gilbert, A.; Baggot, J. Essentials of molecular photochemistry; Blackwell Scientific Publications: Oxford, **1991**; p 265.
36. Schweitzer, C.; Schmidt, R. *Chem. Rev.* **2003**, *103*, 1685.
37. Wu, P.; Brand, L. *Anal. Biochem.* **1994**, *218*(1), 1.
38. Kong, F.; Liu, J.; Zhang, X.; An, Y.; Li, X.; Lin, B.; Qiu, T. *J. Lumin.* **2011**, *131*, 815.
39. Mallick, A.; Haldar, B.; Sengupta, S.; Chattopadhyay, N. *J. Lumin.* **2006**, *118*, 165.
40. Mote, U.; Patil, S.; Bhosale, S.; Han, S.; Kolekar, G. *J. Photochem. Photobiol. B*. **2011**, *103*, 16.
41. Förster, T. Fluoreszenz Organischer Verbindungen; Vandenhueck & Ruprecht: Gottingen, **1951**.
42. Valeur, B.; Berberan-Santos, M. N. Molecular Fluorescence: Principles and Applications; John Wiley & Sons: New York, **2012**.
43. Albani, J. R. Structure and Dynamics of Macromolecules: Absorption and Fluorescence Studies; Elsevier: Oxford, **2011**.
44. Schermann, J.-P. Spectroscopy and Modeling of Biomolecular Building Blocks; Elsevier: Oxford, **2007**.
45. Cury, L.; Bourdakos, K.; Dai, D.; Dias, F.; Monkman, A. *J. Chem. Phys.* **2011**, *134*, 104903.
46. Chen, S.-A.; Lu, H.-H.; Huang, C.-W. In Polyfluorenes; Springer: Berlin, Heidelberg, **2008**.
47. Holt, A.; Leger, J.; Carter, S. *J. Chem. Phys.* **2005**, *123*, 044704.